Insight into LIB diffusion phenomena using analytical impedance models

Eric Woillez, Marion Chandesris

Insight into LIB diffusion phenomena using analytical impedance models

E. Woillez[1] and M. Chandesris[1]

[1]Univ. Grenoble Alpes, CEA, Liten, F-38000 Grenoble, France

Abstract

Electrochemical impedance spectroscopy (EIS) is extensively used to characterize the transport properties in porous electrodes of lithium-ion batteries (LIB). In the low-frequency domain ($f < 1$Hz), solid diffusion and electrolyte diffusion are competing over similar timescales, which explains why both phenomena are difficult to characterize independently. In which case can the solid diffusion coefficient be correctly extracted from experimental EIS? To answer this question, the linearized P2D-Newman model of a complete cell is solved using a Fourier transform to obtain a physics-based analytical impedance. The solution allows deriving the characteristic frequencies and non-dimensional numbers of the system, and gives the parameters range for which solid diffusion is overwhelming electrolyte transport in the impedance signal. A simple criterion is then given to discriminate electrodes that are properly designed for active materials electrochemical characterization.

1 Introduction

The pioneering work of Newman and Doyle in the 90's has laid the fundamentals of what is now called the pseudo-2D (P2D) model of porous electrodes [1, 2, 3, 4]. This model has long become the reference for modeling electrochemical power sources at the electrode scale, especially lithium-ion batteries (LIB). Based on the volume averaging method [5], the model proposes a simplification of the complex 3D porous microstructure using an effective description of electrolyte transport in the electrode depth coupled to representative solid particles for lithium storage. The success of the model lies on the fact that it includes all the leading order transport phenomena and electrochemical reactions in the cell, and, at the same time, remains simple enough to be numerically simulated with very few computational power. However, the model still contains about 16 physical and geometrical parameters (10 per electrode and 6 for the electrolyte) in its simplest version. Almost all of them have to be precisely characterized for the model to correctly predict the battery performances in various conditions, i.e. charge and discharge at small and large regimes.

Among the most difficult parameters to determine are the solid and electrolyte diffusion coefficients. Indeed, these are kinetic parameters that can only be characterized out of equilibrium with relatively long time measurements, from a few minutes to a few hours depending on the active materials and electrolyte transport properties. The idea is thus to design dedicated electrochemical experiments in the vicinity of a given equilibrium state, with applied cell voltage or current that is large enough to get a significant signal, but small enough to avoid non-linear phenomena and parasitic reactions that could occur in the measurement meantime. The galvanostatic intermittent titration technique (GITT) consists in the application of small amplitude pulses of constant current. The solid diffusion coefficient can be deduced from the short or long time overpotential variations [6, 7, 8, 9, 10]. However, the results can be difficult to interpret when the stoechiometry variations during the pulse lead to significant changes in the OCV derivative, or when the active material kinetic properties - such as the charge transfer resistance and the diffusion coefficient - strongly depends on stoechiometry. Another issue is that the double-layer capacitive timescale can become so large at low temperature such as perturbing the diffusive part of the GITT signal. In those conditions, GITT and electrochemical impedance spectroscopy (EIS) analyses have thus to be mixed in order to correctly identify the characteristic respective timescales of interface kinetics and diffusion [11]. Indeed, EIS is extensively used to characterize the transport properties in porous electrodes of lithium-ion batteries (LIB), as it allows to separate high frequency phenomena related to solid-electrolyte interface kinetics and electrolyte

conductivity, from low frequency phenomena related to diffusion [12, 13, 14]. Whereas the high frequency part of experimental EIS (typically $f > 1$Hz) is now well understood thanks to the transmission line model (TLM) first introduced by de Levie [15, 16], the interpretation of the low-frequency part ($f < 1$Hz) is still strongly debated in the electrochemical community [17, 18] One reason is that experimental EIS data are still mostly interpreted using analytical "Warburg" expressions [19] for semi-infinite linear diffusion with either transmissive or reflective boundaries [20] in which solid and electrolyte diffusion are decoupled [21]. Whereas this decoupling approximation is exact in the case of solid thin-film electrodes, it is no longer valid for porous electrodes where both diffusion phenomena are strongly coupled.

A major progress for EIS understanding has been reached when the analytical solution of the linearized P2D model for LIB has been derived [22, 23, 24]. This resolution gives a physics-based model of porous electrodes that includes and extends the one proposed by de Levie, to interpret the whole frequency domain of EIS, and not just the high-frequency part. More recently, a theoretically consistent framework has been proposed to interpret impedance data of electrochemical devices such as capacitors, electrolyte fuel cells, and Li-ion batteries [34, 25, 26]. Such analytical models take into account various properties of electrodes active particles such as the presence of solid electrolyte interphase (SEI) [34], the porous structure of secondary active particles [34], and the non-uniform size distribution of active particles [25]. As already noticed by those authors, there is no simple equivalent electric circuit for the EIS low frequency part, because solid diffusion and electrolyte diffusion are fully coupled over similar timescales and cannot be represented by a few resistance-capacitor elements in series. In the particular case of secondary active particles, it has been shown that the electrolyte diffusion inside the particle pores interfere with the solid diffusion in the low-frequency range of EIS [34]. However, the coupling between solid diffusion and electrolyte diffusion in the electrode porous microstructure has not been fully investigated.

The aim of the present work is to take advantage of the analytical solution of the P2D model to propose a simple framework to interpret the low-frequency part of LIB EIS data. In particular, a criterion will be given to discriminate in which configuration the solid diffusion coefficient can be measured, and in which configuration electrolyte diffusion is overwhelming in the EIS signal. The paper is structured as follows.

We first recall the framework of the linearized P2D model and the method to derive the analytical impedance solution in section 2. The full set of equations and the computational details are postponed in appendices. We then show in section 3 that the studied electrode impedance model is fully characterized by only 3 non-dimensional numbers, 3 characteristic frequencies, and one resistance, given in Table 1. This reduction of the complex 16 parameters initial model to the 7 parameters analytical expression is the crucial step to classify the different EIS phenomenologies. Sections 4 and 5 are a detailed discussion of the possible EIS approximations by the TLM model and by Warburg elements. It is shown in particular that, whereas the high-frequency EIS part can be accurately represented by the TLM model, the low-frequency part has no simple equivalent electric circuit approximation, valid in the general case. In the case where electrolyte diffusion can be neglected, the simple analytical expression [27, 25] called "distributed particle impedance model" in the present work, is recovered, and gives an exact EIS representation. In the reverse case where solid diffusion can be neglected, a capacitive approximation can be given. Unfortunately, none of those approximations are enough to represent the fully coupled model. It is finally shown in section 6 that the LIB spectra in the low-frequency range can be classified in four main classes, depending on the relative weights of two non-dimensional numbers N_s and N_{el}, and two characteristic frequencies f_s and f_{el} related to diffusion phenomena. The Fig. (6) summarizes this result. The simple criterion

$$N_s \gg N_{el}$$

with N_s and N_{el} given in Table 1 in terms of the LIB physical parameters, allows to discriminate the cells where the solid diffusion coefficient can be measured using EIS.

2 System and resolution methodology

We consider a LIB cell composed of a positive porous electrode facing a negative porous electrode. The two electrodes are separated by a porous separator. The active materials are composed of identical spheres of radius r homogeneously distributed inside the electrodes. The system is represented in Fig. (1). Lithium transport is described by a standard P2D-Newman model without thermal nor mechanical effects. Inactive

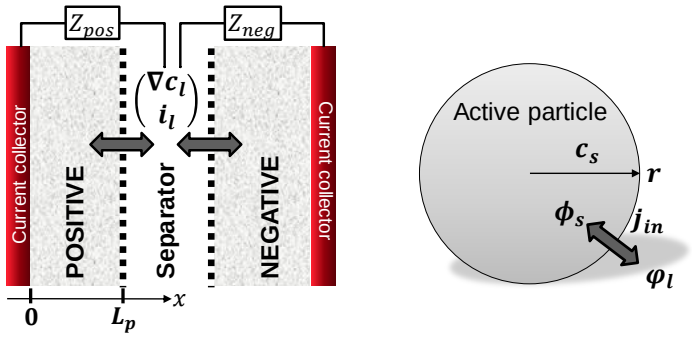

Figure 1: Schematic description of the system. **Left:** the LIB cell is composed of a positive porous electrode with its current collector, facing a negative porous electrode. The two electrodes are separated by a porous separator. The three layers are coupled by charge and mass transport in the electrolyte. **Right:** the active electrode material is represented by identical spheres of radius r, homogeneously distributed in the electrode.

materials volume fraction is neglected in the present study. Moreover, as the electronic conductivity is usually much higher (of the order of 10^5 S/m for graphite, and 600 S/m for the carbon additives of the positive [28]) than the ionic conductivity in the electrolyte, the electric conductivity is considered as infinite in the present model, which implies that the electric potential does not depend on space. The electrolyte transport equations are given by the concentrated solution theory. An electric double layer is considered at the active particle interface, and the lithium insertion in the particle is described by the Butler-Volmer equation. An electrodeposition such as a solid electrolyte interphase (SEI) at the anode or a surface film at the cathod [35] is not considered in the present study. The full equation set of the P2D-Newman model is given in appendix A.

The experimental impedance measurements are usually performed by applying a very small oscillating cell tension, of the order of a few mV, starting from an equilibrium state. In this weak stimulation regime, the non-linearity of the P2D-Newman model can be neglected and the linear equations give a very accurate description of lithium transport. Following the pioneer work of Sikha and White [24] and the more recent developments of [25], we linearize the P2D equations around an equilibrium state and we solve them in the frequency domain. The result is a formal expression of the LIB cell impedance in terms of the P2D parameters. The analytical expression can then be evaluated much faster than a simulation of the P2D model for an applied oscillating tension. As the derivation of the analytical expression is quite cumbersome, we postpone the full development to appendix E, and we only give below the different steps. The notations used in the present paper are given in appendix A and B.

1. The solid diffusion equation in the active particles, and the double-layer charging equation are solved independently in appendix C, to obtain the particle impedance $Z_{part}[\Omega.\mathrm{m}^2]$ defined by the relation

$$(j_{out} + j_{dbl})\, Z_{part} = \phi - \varphi_l \tag{1}$$

   The full expression of Z_{part} is given by Eq. (36) in the appendix. Z_{part} should be interpreted as the impedance relating the local current density $j_{out} + j_{dbl}$ flowing outward the particle and the interface overpotential $\phi - \varphi_l$.

2. A time Fourier transform is applied to the linear set of transport equations in the electrolyte, and the system is then completely written with non-dimensional variables and parameters. The result is given by Eqs. (44-45) in appendix D.

3. The difficult step achieved in section E is the resolution of the two coupled equations of charge and mass transport in the electrolyte. This is done by decomposition of the solution vector (c_l, i_l) in eignenmodes. The concentration and current density fields can then be expressed in terms of the boundary conditions

(C_l, J) at the electrode/separator interface located at $x = L$, and the eigenvector matrix M via

$$\begin{pmatrix} c_l(x) \\ i_l(x) \end{pmatrix} = M(x).M^{-1}(L).\begin{pmatrix} C_l \\ J \end{pmatrix}$$

The expression of M is given in Eqs. (50-52). This is done for the positive and negative porous electrodes.

4. The unknown concentrations C_l at each interface can be found by the continuity relations for mass transport, namely by enforcing the continuity of the flux $-D_l^{\text{eff}}\nabla c_l$ at each interface. This is done in Eqs. (57).

5. Finally, once the fields $c_l(x)$ and $i_l(x)$ are known, the electrode potential drop can be computed in terms of the eigenmode matrices and the interface concentrations using the relation between i_l and the potentials given in Eq. (1). The expressions are given in Eqs. (58-59). The potential drop inside the separator is also included in the total impedance in Eqs. (60-61).

The output of the analytical computation provides the positive impedance Z_{pos} [Ω.m^2] in Eq. (60), obtained from the potential drop between the positive current collector and the middle of the separator, and Z_{neg} [Ω.m^2] in Eq. (61), obtained from the potential drop between the middle of the separator and the negative current collector (see Fig. 1). We strongly emphasize that the final expression is not trivial. Because of the mass transport equation in the electrolyte, the impedance of a stack composed of a positive electrode, a separator and a negative electrode cannot be written as the sum of the impedances of each layer. This in particular means that the equivalent electrical circuits composed of Warburg elements often used in the literature to model a LIB cell impedance are *in general* only approximations, as they cannot fully account for mass and charge coupling in the electrolyte. One purpose of the present paper is to study in which limiting cases or with which accuracy can a LIB cell impedance be represented by an equivalent electric circuit.

3 Characteristic frequencies and non-dimensional numbers

The P2D-Newman model described in appendix A has 10 parameters per electrode and 6 for the electrolyte, that are summarized in the Tables 3 and 4. It is therefore an outstanding challenge to determine the respective model sensitivity to each parameter. The great advantage of reducing the model to its non-dimensional set of equations is to explicitly display the characteristic timescales and non-dimensional numbers associated to the different transport phenomena in the porous electrode. The P2D model detailed in appendix A takes three transport mechanisms into account, namely lithium transfer at the interface with double-layer charging (high frequency phenomenon), the lithium transport in the solid phase by diffusion, and the lithium ionic transport by conduction and diffusion in the electrolyte. The solid and electrolyte diffusions are low-frequency phenomena. In case where the Nernst-Einstein relation (Eq. (5) with $\alpha_l = 1$) is satisfied, the full analytical derivation done in appendix shows that the impedance of a porous electrode only depends on 3 characteristic frequencies, 3 non-dimensional numbers, and one characteristic resistance $\mathcal{Z}$ that gives the impedance order of magnitude. When the Nernst-Einstein relation is not satisfied, an additional non-dimensional parameter α_l has to be introduced, that somewhat breaks the beautiful equations symmetry. However, as α_l is usually close to one in standard electrolytes, this non-dimensional number does not strongly impact the final impedance value and its effect can be included in the non-dimensional ionic diffusion number. This means that each transport phenomenon can be naturally associated to one characteristic frequency and one non-dimensional number. Their explicit expression with respect to the P2D set of parameters are given in Table 1. In the following, we discuss in more details the three mechanisms.

	Solid diffusion	Electrolyte diffusion	Electrochemical (fast) kinetics
Characteristic frequencies	$f_s = \frac{D_s}{r^2}$	$f_{el} = 2\alpha_l \left(1 + \frac{\partial \ln \gamma}{\partial \ln c}\right) \frac{j_0 S_a t^+ (1-t^+)}{2\pi F c_0 \varepsilon}$	$f_{capa} = \frac{F j_0}{2\pi RT C_{dbl}}$
Non-dimensional numbers	$N_s = \frac{j_0 r \lvert \phi'_{ocv} \rvert}{RT D_s c_s^{max}}$	$N_{el} = 1 + \frac{1-t^+}{\alpha_l t^+}$	$N_\sigma = \frac{\lambda}{L}$
Characteristic electrode resistance	$\mathcal{Z} = \frac{\lambda}{\sigma_l^{\text{eff}}}$ [Ω.m^2]		

Table 1: Characteristic frequencies, non-dimensional numbers, and order of magnitude of a porous electrode impedance, as functions of the P2D-Newman parameters.

Electrochemical kinetics : conductivity, double-layer charging, and insertion

The characteristic frequency f_{capa} and the non-dimensional number N_σ are associated with the high frequency kinetics of the cell. They are displayed in the third column of Table 1. Those numbers are derived from the ionic conductivity, and the solid-electrolyte interfacial kinetics composed of double layer charging and lithium insertion. The frequency f_{capa} can be seen as the typical frequency of a parallel RC equivalent electric circuit, where the capacity is C_{dbl} and the resistance is the standard charge transfer resistance, that is $R_{CT} = \frac{RT}{F j_0}$. The non-dimensional number N_σ is the ratio between the typical penetration length λ and the electrode thickness L, where the penetration length is [16, 29, 30]

$$\lambda = \sqrt{\frac{RT\sigma_l^{\text{eff}}}{F j_0 S_a}} \tag{2}$$

For $f \gg f_{capa}$, the current density decreases exponentially from the electrode surface over a typical depth λ, and N_σ can be interpreted as the electrode fraction where lithium exchange between the electrolyte and the active material effectively takes place. f_{capa} and N_σ are the same as the characteristic frequency and the non-dimensional number that appear in the famous TLM model [16]. This is not by chance, as the TLM model is an excellent approximation of the full P2D-Newman impedance in the high frequency limit when diffusion kinetics can be neglected. The connection between both models is described in more details in section 4. It is worth mentioning that the additional frequency $f_t = f_{capa} N_\sigma^2$ also plays a role in the shape of the high frequency electrode impedance. Its explicit expression is

$$f_t = \frac{\sigma_l^{\text{eff}}}{2\pi S_a C_{dbl} L^2} \tag{3}$$

It corresponds to the characteristic frequency at which the electrode impedance deviates from a 45° line in the high frequency range (see [34]).

Solid diffusion

The resolution of the isotropic diffusion equation in a sphere of radius r (details in appendix C) shows that the impedance of an active particle can be computed independently from the electrolyte diffusion. The solid diffusion effect is fully characterized by a non-dimensional impedance Z_s defined between the lithium flux flowing outside the particle and the overpotential by (see Eq. (33) and refs [31, 8])

$$\begin{aligned} j_{out}\,(1 + Z_s) &= \frac{j_0 F}{RT}\,(\phi - \varphi_l) \\ Z_s &= N_s \frac{\tanh(\sqrt{i\omega/f_s})}{\sqrt{i\omega/f_s} - \tanh(\sqrt{i\omega/f_s})} \end{aligned} \tag{4}$$

where j_{out} is the surface outwards current density, $\phi = \Phi - \phi_{ocv}(x_0)$ is the difference between the electrode potential and the equilibrium OCV, and φ_l is the electrochemical potential of lithium ions. The characteristic frequency f_s and the non-dimensional number N_s associated with lithium isotropic diffusion in a spherical particle of radius r, are displayed in the first column of Table 1. The frequency f_s is typical of diffusive

phenomena, and represents the inverse of the timescale needed for a concentration profile to relax over a domain of size r. The expression of N_s is less intuitive, but some physical aspects can be identified. The non-dimensional number appears from the competition between lithium insertion kinetics and solid diffusion. There is no overpotential associated with solid diffusion if the OCV is flat, because in that case the lithium chemical potential does not change with concentration. This is reflected by the fact that $N_s = 0$ if $\phi'_{ocv} = 0$. It can be also noticed that N_s is proportional to r/D_s, which makes sense because larger particles with a weaker diffusion will enhance the concentration inhomogeneity across the particle and increase the overpotential associated to solid diffusion.

Electrolyte diffusion

The characteristic frequency f_{el} and the non-dimensional number N_{el} associated with ionic diffusion in the porous electrode are displayed in the second column of Table 1. It can be seen that the frequency f_{el} is proportional to $\frac{j_0 S_a}{F c_0 \varepsilon}$, which is the inverse timescale for charge pumping in the electrolyte. When the electrode is charged, the lithium ions are pumped from the pores reservoir, and the counter-ions are moved by the electrochemical potential to ensure electroneutrality. It can be seen in particular that $f_{el} = 0$ if the lithium ions have no mobility (case $t^+ = 0$) or if the counter-ions have no mobility (case $t^+ = 1$). The parameter α_l represents the deviation of the ionic diffusion coefficient from the Nernst-Einstein relation, it is defined by

$$D_l = \alpha_l \frac{2RT\sigma_l}{F^2 c_0} t^+(1 - t^+) \tag{5}$$

Eq. (5) reduces to the Nernst-Einstein relation when $\alpha_l = 1$. It can be shown with the expression of the penetration length Eq. (2) that the electrolyte frequency has the equivalent expression

$$f_{el} = 2\pi \frac{D_l^{\text{eff}} \left(1 + \frac{\partial \ln \gamma}{\partial \ln c}\right)}{\lambda^2 \varepsilon} \tag{6}$$

This latter formulation displays the factor $\frac{D_l^{\text{eff}}}{\lambda^2}$which is the timescale to diffuse over a length λ. This shows more obviously that the porous electrode only "works" over a depth λ.

The number N_{el} has a physical meaning. When a constant current is applied to an electrolyte membrane between two lithium foils, the electrolyte resistance is initially R_0 and increases with time due to electrolyte diffusion to eventually reach an asymptotic value R_∞. This technique is often used to measure the electrolyte transport number [32]. It can be shown that N_{el} gives the multiplicative factor of resistance increase, that is $\frac{R_\infty}{R_0} = N_{el}$. This number only depends on the electrolyte properties, not on the electrode microstructure.

Finally, we note that the expression of the characteristic resistance $\mathcal{Z}$ given in Table 1 is reminiscent of the resistance of a porous membrane, but with a width given by the penetration length λ (in Eq. (2)) instead of the total electrode width L. This again supports the general idea that a porous electrode only works over a depth λ.

The Table 2 gives the values of the characteristic frequencies, non-dimensional numbers and characteristic resistance at 25°C for a NMC positive electrode, and a graphite negative electrode. The parameters used for the numerical application are summarized in Table 3. They correspond to typical values of a NMC vs graphite with a positive loading of 22 mg/cm^2. The values of Table 2 illustrate that a NMC electrode and a graphite electrode have completely different diffusion magnitudes. This is particularly clear because the value of N_s is much larger for the graphite electrode than for the NMC electrode. Moreover, the frequencies f_{el} and f_s are higher for the NMC electrode. Those two observations lead to the conclusion that diffusive transport is much more efficient in the NMC electrode than in the graphite electrode, given the electrode parameters of Table 3. The conclusion is obvious from the values of the characteristic frequencies and non-dimensional numbers of Table 2, whereas it is much more difficult to assert just looking at the full set of P2D parameters of Table 3.

	NMC	Graphite
f_{capa}	100 Hz	10 Hz
f_{el}	3,7 mHz	0,61 mHz
f_s	16 mHz	0,16 mHz
N_σ	0,73	0,81
N_{el}	3,3	3,3
N_s	0,32	11
$\mathcal{Z}$	0,44 mΩ.m^2	1,5 mΩ.m^2

Table 2: Order of magnitude of the characteristic frequencies and non-dimensional numbers for a NMC vs graphite cell at 25°C. The values are computed with the formal expressions given in Table 1.

4 TLM (high frequency) approximation

The TLM model introduced by De Levie [15, 16] has historically been the first physics-based impedance model of porous electrodes, which explains its popularity to interpret the experimental impedance data. Some authors have later shown [27, 25] that the TLM model in fact gives an exact analytical expression for the P2D impedance in the high frequency limit, when liquid and solid diffusion phenomena can be neglected. In the present section, we discuss more precisely the validity conditions of the TLM model.

The TLM impedance is given by [29]

$$\begin{cases} Z_{TLM} &= \dfrac{\lambda\sqrt{\frac{j_0 F}{RT} Z_{int}}}{\sigma_l^{\text{eff}} \tanh\left(\frac{L}{\lambda\sqrt{\frac{j_0 F}{RT} Z_{int}}}\right)} \\ Z_{int} &= \frac{R_{CT}}{1+i\frac{\omega}{2\pi f_{capa}}} \end{cases} \tag{7}$$

with the specific double-layer charging frequency f_{capa} given in Table 1 and the charge transfer resistance $R_{CT} = \frac{RT}{Fj_0}$. Z_{int} corresponds to the individual particle impedance when solid diffusion is neglected. The TLM impedance given by Eq. (7), corrected by the separator resistance $\frac{L_s}{\sigma_{sep}^{\text{eff}}}$, is displayed in Fig. (2) for the positive NMC electrode and the negative graphite electrode, in the frequency range 10 kHz $< f <$ 1 Hz. By comparison, the exact analytical impedance is displayed with the blue curve. It can be seen in Fig. (2) that the TLM approximation indeed becomes exact in the high frequency limit, and that the approximation is very good all over the high-frequency domain $f >$ 1 Hz.

The TLM model is based on the assumption that all diffusion transport mechanisms, in the electrolyte and in the solid phase, are negligible. This is indeed the case if the diffusion takes place over much longer timescales than the double-layer charging. This can be mathematically expressed as

$$\begin{cases} f_{el} &\ll f_{capa} \\ f_s &\ll f_{capa} \end{cases} \tag{8}$$

with the frequencies f_{el} and f_s given in Table 1. The exact resolution of the P2D impedance for the NMC - graphite cell shows that the main correction to the TLM comes from the solid diffusion. As the solid diffusion impedance is much larger for the graphite electrode than for the NMC electrode, a small deviation from the TLM model can be seen in the blue curve of Fig. (2) right. A more complex expression to take solid diffusion into account is proposed in section 5.

The electrolyte diffusion in the separator may also contribute to the high-frequency part of the impedance. Indeed, a characteristic frequency for diffusion in the separator is given by

$$f_{sep} = \frac{D_{sep}^{\text{eff}}}{L_s^2},$$

which gives $f_{sep} \approx$ 50 mHz for a 16 μm separator of Mcmullin number 8. In the present configuration $f_{sep} \ll f_{capa}$, which also justifies that the diffusive phenomena inside the separator can be neglected.

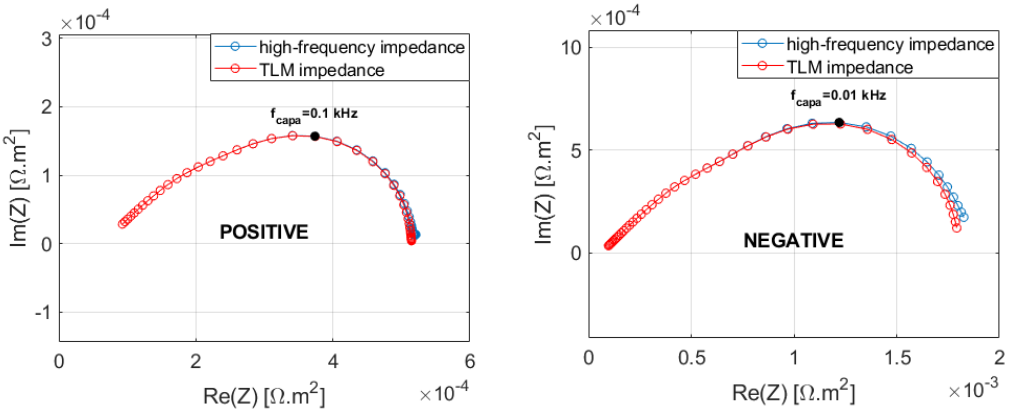

Figure 2: High-frequency impedances (10 kHz $< f <$ 1 Hz) of the positive (left) and negative (right) electrodes for a NMC vs graphite cell at 25°C. The blue curve displays the impedance obtained with the P2D-Newman model, and the red curve displays the TLM approximation corrected by the separator resistance, that is $Z = Z_{TLM} + \frac{L_s}{2\sigma_{sep}^{\text{eff}}}$.

5 Contribution of diffusion phenomena

The present section is devoted to the investigation of the solid diffusion and the electrolyte diffusion respective contributions to the low-frequency part of the cell impedance. The aim is to emphasize the phenomenology related to one or the other diffusion phenomenon. For that purpose, we will first deal with the limit of negligible electrolyte diffusion, then with the reverse limit of negligible solid diffusion, and finally with both fully coupled diffusion phenomena.

Negligible electrolyte diffusion

A negligible electrolyte diffusion would correspond to the asymptotic limit $t^+ \to 1$. In that case, the counter-ions have a vanishing mobility and the lithium ions concentration profile cannot be distorted because it would break electroneutrality. The limit $t^+ \to 1$ guarantees a uniformly flat concentration profile in the model, without any electrolyte diffusion, while keeping a non-negligible electrolyte conductivity. In this limit, both half-cells are decoupled such that the positive and the negative impedances can be computed separately as shown in appendix F. The exact analytical P2D impedance of the half-cell reduces to the simple expression

$$Z = Z_{DP} + \frac{R_{sep}}{2} \tag{9}$$

with

$$\begin{cases} Z_{DP} &= \dfrac{\lambda\sqrt{\frac{j_0 F}{RT} Z_{part}}}{\sigma_l^{\text{eff}} \tanh\left(\frac{L}{\lambda\sqrt{\frac{j_0 F}{RT} Z_{part}}}\right)} \\ Z_{part} &= \dfrac{R_{CT}}{\frac{1}{1+Z_s} + i\frac{\omega}{2\pi f_{capa}}} \end{cases} \tag{10}$$

with the solid diffusion impedance Z_s given by Eq. (4), and

$$R_{sep} = \frac{L_s}{\sigma_{sep}^{\text{eff}}} \tag{11}$$

The impedance Z_{DP}, already introduced by [25], is called "distributed particle impedance", because it takes into account the non-uniform distribution of currents, potentials and solid concentration in the electrode depth. Looking at Eqs. (7) and (10), one can see that the distributed particle impedance is a natural

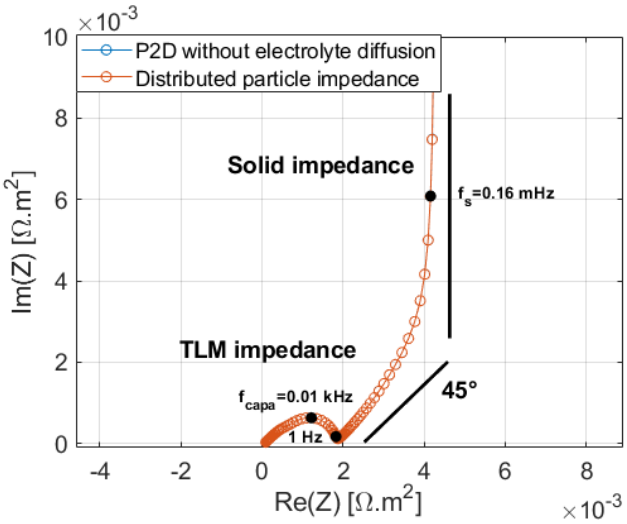

Figure 3: Illustration of the solid diffusion contribution to the low-frequency impedance of the negative electrode. The frequency range is 0,1 mHz $< f <$ 10 kHz. The exact P2D impedance in the vanishing electrolyte diffusion limit ($t^+ = 1$) in blue, and the distributed particle impedance model given by Eqs. (9-10) in red, are superimposed. The impedance is typical of a blocking diffusion impedance, with a 45° line for short-time diffusion, followed by a vertical line when the solid diffusion profile has time to stabilize. The transition between the two regimes typically occurs around the frequency f_s.

extension of the TLM impedance where the single particle impedance contains both double-layer charging and solid diffusion. Both the P2D impedance with vanishing electrolyte diffusion and the distributed particle impedance of Eq. (9) are displayed in Fig. (3): the two curves are indistinguishable.

The Fig. (3) shows that the high-frequency part given by the TLM impedance smoothly joins the low-frequency part where solid diffusion takes place. The solid diffusion impedance is typical of a blocking diffusive impedance. It is composed of a 45° tilted line for short timescales where diffusion has no time to reach the center of the active particle, and it is followed by a vertical line that means that diffusion has reached a stationary state and lithium insertion is blocked. The transition between both regimes occurs at the typical frequency f_s given in Table 1.

Negligible solid diffusion

We now turn to the other limit where solid diffusion is negligible and the low frequency part of the impedance is dominated by electrolyte diffusion. This limit can be achieved e.g when $\phi'_{ocv} = 0$, because in that case the concentration gradient in the active particle does not create any overpotential. Contrary to the previous limiting case, the electrolyte diffusion impedance is not given by a simple TLM-like expression. The exact analytic expression can only be achieved by solving the full charge and mass transport coupling in the electrolyte, as done in appendix E. The exact P2D impedance without solid diffusion is displayed in blue in Fig. (4) for both electrodes. The impedance shape begins with the TLM curve at high frequency ($f >$ 1Hz), and is followed by the electrolyte diffusion impedance at low frequency ($f <$ 1Hz). This latter is a passing impedance, that means, it has a finite resistance in the limit $f \to 0$.

The Fig. (4) moreover shows that the electrolyte impedance very closely looks like a semi-circle, especially for the negative impedance. It is therefore different from the transmissive Warburg impedance of an electrolyte membrane between two thin-film electrodes [21, 14] that displays a 45° straight line. The diameter R_l of this pseudo semi-circle can be computed exactly from the vanishing frequency limit $f \to 0$, as shown in appendix G. This observation prompts to propose the following electric circuit approximation in the form of a RC impedance:

$$Z = Z_{TLM} + \frac{R_{sep}}{2} + Z_{RC} \tag{12}$$

with

$$\begin{cases} Z_{RC} &= \frac{R_l + \frac{R_{sep}(N_{el}-1)}{2}}{1+i\frac{\omega}{2\pi f_{el}}} \\ R_l &= \frac{\lambda}{\sigma_l^{\text{eff}}} \left(\frac{\sqrt{N_{el}}}{\tanh\left(\sqrt{N_{el}}\frac{L}{\lambda}\right)} - \frac{1}{\tanh\left(\frac{L}{\lambda}\right)} \right) \end{cases} \tag{13}$$

and the non-dimensional electrolyte number N_{el} given in Table 1. Note that R_l is a pure resistance and does not depend on ω. The approximation given by Eqs. (12-13) is displayed with the red curves in Fig. (4). We strongly emphasize that the simple expression given by Eq. (12) is an approximation, not the exact P2D analytical impedance. The limits of this expression have thus to be discussed.

The expression of Eq. (12) is based on the implicit assumption that the TLM impedance is in serie with the RC approximation of the electrolyte impedance. This can only be justified if both phenomena are decoupled by a clear time-scale separation, that is $f_{el} \ll f_{capa}$. The strength of Eq. (13) is that it gives the correct asymptotic resistance in the limit $f \to 0$, as can be seen in Fig. (4). In Eq. (13), f_{el} is exactly the RC frequency, and is thus located on the top of the RC semi-circle impedance (red curve). In the P2D impedance (blue curve), the whole system, positive electrode, separator, and negative electrode is fully coupled by mass transport in the electrolyte. The characteristic frequency f_{el} is not exactly located at the point of maximal imaginary part (top of the pseudo semi-circle). It can be located slightly on the left of the imaginary part maximum - as for the positive - or slightly on the right of the imaginary part maximum - as for the negative. The deviations are due to the reciprocal influence of both electrode impedances on each other. Besides, expression (13) can only be used if the separator is very thin compared to the electrodes, such that its own timescale has no impact on the whole impedance.

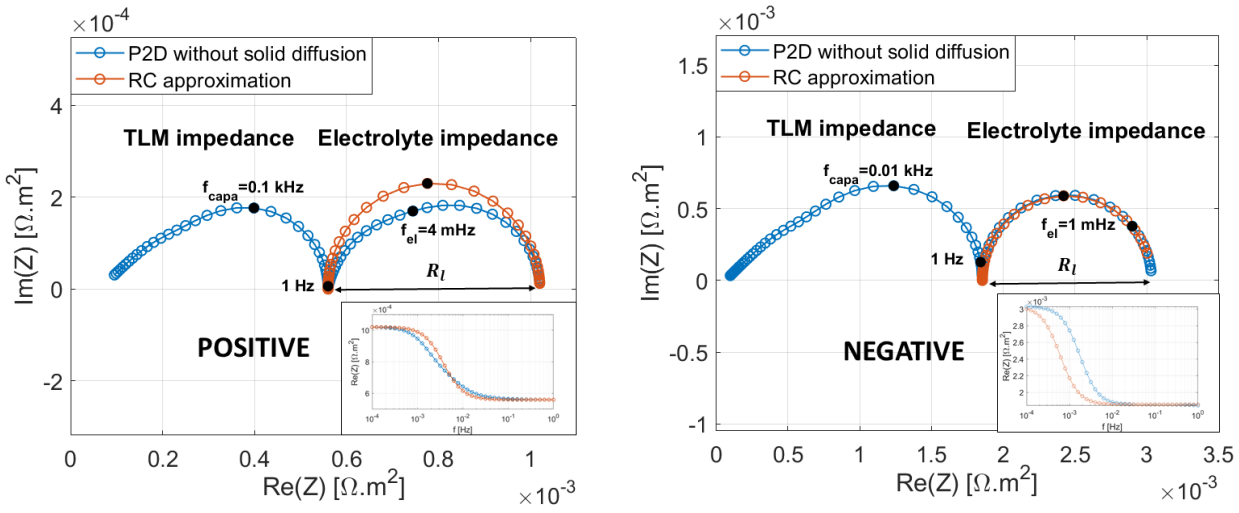

Figure 4: Illustration of the electrolyte diffusion contributions to the low-frequency impedance of the positive (left) and the negative (right) electrodes. The frequency range is 0,1 mHz $< f <$ 10 kHz. The electrolyte diffusion part is close to a semi-circle with characteristic frequency f_{el} (given in Table 1). The blue curve represents the exact P2D impedance without solid diffusion ($\phi'_{ocv} = 0$) and the red curve represents the RC approximation given by Eqs. (12-13). The inset panels display the impedance real part in the low frequency range $f <$ 1 Hz.

Coupled diffusion phenomena

Finally, the Fig. (5) displays the electrolyte impedance (in blue), the distributed particle impedance (in orange) and the exact P2D full impedance (in red) for the positive and the negative electrodes. It can be seen that the phenomenology of the low-frequency impedance strongly differs for both electrodes.

For the positive electrode, the low-frequency part is mainly a vertical straight line created by the blocking solid diffusion, that is slightly tilted by the contribution of the electrolyte impedance. For this electrode, the tilted straight line should not be interpreted as the solid diffusion 45° line, because its angle is entirely set by

the electrolyte diffusion, and not by solid diffusion. For the negative electrode on the contrary, solid diffusion can be clearly identified at the beginning of the low-frequency impedance. The impedance is very close to a 45° straight line characteristic of solid diffusion. It is only slightly above the solid diffusion because the electrolyte impedance gives a small imaginary contribution for $f > f_{el}$. For $f < f_{el}$, the electrolyte diffusion equilibrates and the full impedance is slightly shifted to the right compared to the solid diffusion impedance.

The Fig. (5) (purple stars) also displays the equivalent electric circuit impedance given by

$$Z = Z_{DP} + Z_{RC} + \frac{R_{sep}}{2} \tag{14}$$

with the distributed particle impedance given by Eq. (10) and the RC-approximated impedance for electrolyte diffusion given by Eq. (13). It can be seen that the equivalent electric circuit impedance is a relatively poor approximation of the exact P2D impedance. The first reason is that the impedance Z_{RC} is only an approximation of the electrolyte diffusion impedance, and the second reason is that the exact impedance is not the sum of the solid diffusion impedance and the electrolyte diffusion impedance. Instead, both diffusive phenomena are coupled and distributed in the depth of the porous electrode. The equivalent electric circuit impedance Eq. (14) can only be used to obtain orders of magnitudes of diffusive phenomena in the low-frequency range, but the proper extraction of transport parameters for impedance data should be done with the full P2D expression.

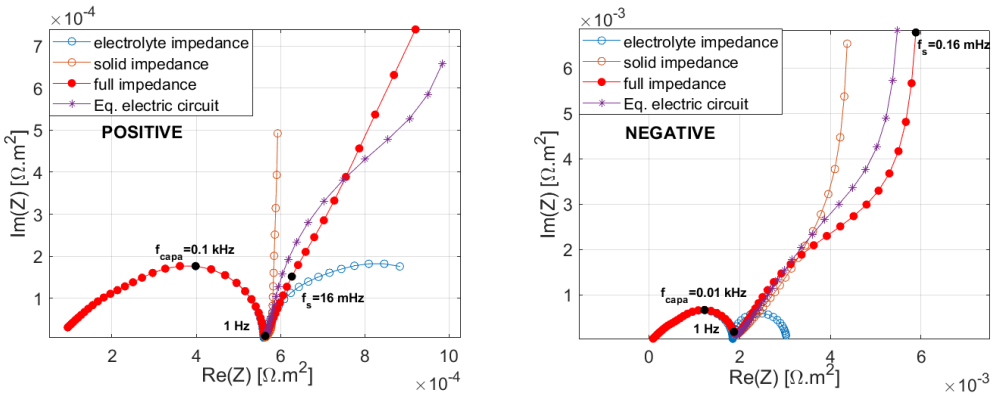

Figure 5: Impedance spectra of the positive (left) and negative (right) electrodes of a NMC vs graphite cell at 25°C obtained with the P2D-Newman model. The frequency ranges are 1,6 mHz $< f <$ 10 kHz for the positive, and 0,16 mHz $< f <$ 10 kHz for the negative. The blue curve displays the electrolyte contribution (obtained with $\phi'_{ocv} = 0$), the orange curve displays the solid diffusion contribution (obtained with $t^+ = 1$) and the red curve displays the full model impedance.

6 Low frequency phenomenology

It has been shown in section 3 that the impedance phenomenology of a porous electrode is entirely determined by 3 non-dimensional numbers and 3 frequencies (see Table 1). Most often, the frequency f_{capa} that characterizes the double-layer charging and charge transfer is much higher than the characteristic frequencies of diffusion phenomena. For this reason, the impedance displays two distinct frequency domains: the high frequency part (1Hz$< f$) is dominated by the double layer charging, whereas the low-frequency part ($f <$1Hz) is dominated by the solid and electrolyte diffusions.

The low-frequency impedance phenomenology can thus be classified according to the 2 non-dimensional numbers N_s and N_{el}, and the 2 frequencies f_s and f_{el}. Depending on the relative magnitudes of those four quantities, the low-frequency impedance may displays four different phenomenologies that are summarized in Fig. (6). We describe below each of this phenomenology in more details.

Overwhelming solid diffusion, case $N_{el} \ll N_s$ and $f_{el} \ll f_s$ according to the LFP parameters of Table 3. The electrolyte diffusion magnitude is much lower than the solid diffusion magnitude, and happens on

much longer time-scales. The low-frequency impedance part is thus very close to an ideal solid diffusion impedance, with a 45° straight line followed by an almost vertical line when solid diffusion becomes blocking. This behaviour can be encountered for example for LFP-type positive electrodes where the OCV is very steep ($\phi'_{ocv} \approx 10$V outside the phase transition plateau) and the solid diffusion coefficient is very low ($D_s \approx 10^{-16}\text{m}^2/\text{s}$). This is the ideal configuration to measure the solid diffusion coefficient by fitting the impedance data.

Transient solid diffusion, case $N_{el} \ll N_s$ and $f_s \ll f_{el}$ according to the graphite parameters of Table 3. The electrolyte diffusion magnitude is much lower than the solid diffusion magnitude, but happens on much shorter time-scales. The consequence is a low-freqency impedance close, but slightly above a 45° line characteristic of solid diffusion. This phenomenology can be encountered in graphite electrodes where the particles are quite large ($r \approx 8\mu$m). The solid diffusion coefficient can still be measured, provided the model used to fit the impedance data correctly takes into account electrolyte diffusion.

Blocking solid diffusion, case $N_s \ll N_{el}$ and $f_{el} \ll f_s$ according to the NMC parameters of Table 3. The electrolyte diffusion magnitude is much larger than the solid diffusion magnitude, and happens on much longer time-scales. For frequencies smaller than f_s, the solid diffusion is in the blocking limit and contribute with a vertical line to the low-frequency impedance. The impedance line is tilted compared to the vertical because of electrolyte diffusion correction. This behaviour can be observed in NMC electrodes where solid diffusion has a negligible contribution to the total overpotential compared to the other kinetic phenomena. The solid diffusion coefficient cannot easily be measured with the impedance data, but information on the electrolyte can be obtained using the deviation from the vertical line.

Overwhelming electrolyte diffusion, case $N_s \ll N_{el}$ and $f_s \ll f_{el}$. To obtain this impedance, the NMC parameters of Table 3 and the electrolyte parameters of Table 4 have been modified using $\frac{\partial \ln \gamma}{\partial \ln c} = 3$, $r = 5$ μm, and $D_s = 5.10^{-14}\text{m}^2/\text{s}$. The electrolyte diffusion magnitude is much larger than the solid diffusion magnitude, and happens on much shorter time-scales. The low-frequency impedance is mainly described by the passing electrolyte diffusion impedance, with a superimposed solid diffusion correction. It can be seen in the bottom right panel of Fig. 6 that the solid diffusion contribution only becomes significant below f_s where the impedance switch from the passing to the blocking behaviour. This configuration can not be easily encountered with porous electrodes composed of standard active materials and electrolyte. This type of impedance could be used to measure the electrolyte transport properties rather than the solid diffusion coefficient.

7 Conclusion

We have presented an analytical solution of the linearized P2D-Newman model for complete cells of Li-ion batteries in the frequency domain. We have shown the link between this exact solution and some of the analytical approximations previously reported in the literature, in particular with the de Levie model [15] and the distributed particle impedance model [27]. For the electrolyte contribution, we have shown that the impedance in a porous electrode is different from the transmissive Warburg impedance and we alternatively propose an equivalent RC approximation. The resolution shows that the EIS can be written in terms of three non-dimensional numbers, three characteristic frequencies, and one characteristic resistance. In the low frequency domain (typically for $f < 1$Hz), the EIS is dominated by solid and liquid diffusion phenomena. They are respectively associated to two non-dimensional numbers (N_s, N_{el}) and two characteristic frequencies (f_s, f_{el}). The major result of the paper is then to show that the low frequency EIS phenomenology can be classified in four different configurations, depending on the relative weights of N_s and N_{el} on the one hand, and of f_s and f_{el} on the other hand (see Fig. (6)).

As a result, it is not always possible to use EIS data to measure the solid diffusion coefficient because solid diffusion can be overwhelmed by electrolyte diffusion at low frequencies. More precisely, the present work proposes a framework to design porous electodes in which the solid and electrolyte diffusions can be decoupled in the EIS signal, using the comparison of the two non-dimensional numbers N_s and N_{el}. The solid diffusion coefficient can be measured only if $N_s \gg N_{el}$, whereas the electrolyte diffusion coefficient can

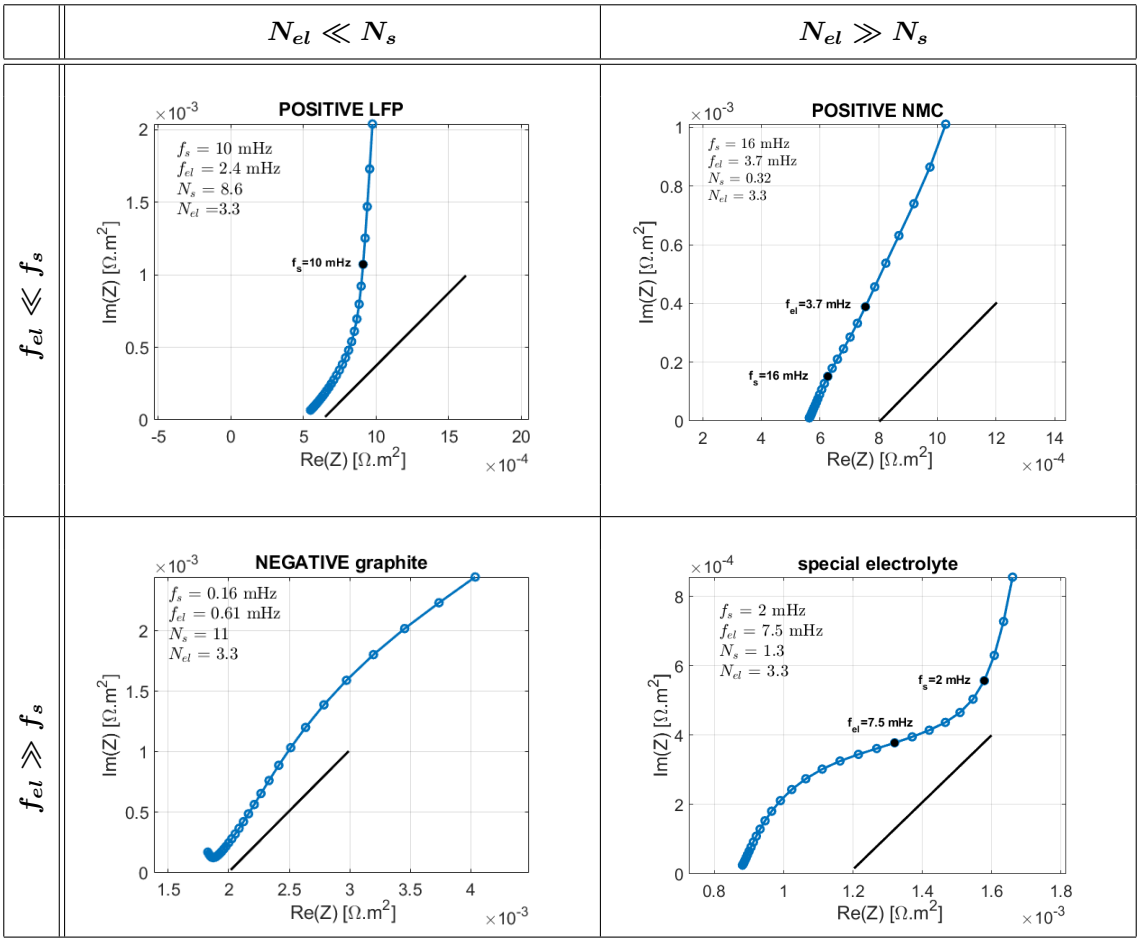

Figure 6: The four possible phenomenologies for the low-frequency impedance of LIB porous electrodes. The black thick line represents a 45° slope. **Top left** : a LFP-type impedance where solid diffusion dominates, in the range 1Hz-5mHz. **Bottom left** : a graphite-type impedance where solid diffusion is mixed with electrolyte diffusion, in the range 1Hz-1mHz. **Top right** : a NMC-type impedance where solid diffusion is mixed with electrolyte diffusion, in the range 1Hz-1mHz. **Bottom right** : a NMC-type impedance with large electrolyte activity, where electrolyte diffusion dominates, in the range 1Hz-1mHz.

be measured only if $N_{el} \gg N_s$, which gives an easy criterion to interprete the EIS low-frequency part. A major perspective is to be able to apply the present theory to real porous electrodes, and measure solid and electrolyte diffusion kinetics with different electrode designs : this experimental work will be done in a future paper.

The present work has focused on full cells with two porous electrodes probed with an ideal reference electrode located at the middle of the separator. In this configuration, both electrodes are weakly coupled by the transport in the electrolyte, which justify the independent analysis of each electrode. For half-cells studies, porous electrode facing Li-metal foil, the non-dimensional numbers and characteristic frequencies will remain the same for the porous electrode. However, the coupling between the two electrodes is stronger and might lead to a different phenomenology than the one reported in the present work. SEI and cathodic surface films films are not considered in the present work but can be taken into account using a modification of the one-particle impedance defined by the relation Eq. (1). The SEI film can have a large impact on the electrode impedance, as shown in ref. [34]. However, its effect is almost completely limited to the high-frequency part and cannot interfere with the electroyte nor solid diffusion signatures.

The P2D-Newman model studied in the present paper only considers Fick's law for lithium transport in the active materials. A point that is actively discussed in the battery community is to know whether this simple law can also account for materials displaying phase transitions such as LFP or graphite. A natural extension of the present work is to propose a full analytical solution for EIS model including phase transition, that is still lacking in the literature.

References

[1] Doyle M, Fuller T F and Newman J 1993 *Journal of the Electrochemical society* **140** 1526

[2] Fuller T F, Doyle M and Newman J 1994 *Journal of the electrochemical society* **141** 1

[3] Doyle M, Newman J, Gozdz A S, Schmutz C N and Tarascon J M 1996 *Journal of the Electrochemical Society* **143** 1890

[4] Newman J and Thomas-Alyea K E 2012 *Electrochemical systems* (John Wiley & Sons)

[5] Whitaker S 1998 *The method of volume averaging* vol 13 (Springer Science & Business Media)

[6] Weppner W and Huggins R A 1977 *Journal of The Electrochemical Society* **124** 1569

[7] Wen C J, Boukamp B A, Huggins R A and Weppner W 1979 *Journal of The Electrochemical Society* **126** 2258–2266

[8] Subramanian V R, Ritter J A and White R E 2001 *Journal of The Electrochemical Society* **148** E444

[9] Dees D W, Kawauchi S, Abraham D P and Prakash J 2009 *Journal of Power Sources* **189** 263–268 ISSN 0378-7753

[10] Delacourt C, Ati M and Tarascon J 2011 *Journal of the Electrochemical Society* **158** A741

[11] Nickol A, Schied T, Heubner C, Schneider M, Michaelis A, Bobeth M and Cuniberti G 2020 *Journal of The Electrochemical Society* **167** 090546

[12] Orazem M and Tribollet B 2017 *Electrochemical Impedance Spectroscopy* 2nd ed (John Wiley & Sons)

[13] Meddings N, Heinrich M, Overney F, Lee J S, Ruiz V, Napolitano E, Seitz S, Hinds G, Raccichini R, Gaberscek M and Park J 2020 *Journal of Power Sources* **480** 228742 ISSN 0378-7753

[14] Vivier V and Orazem M E 2022 *Chemical Reviews* **122** 11131–11168 pMID: 35687869 (*Preprint*)

[15] De Levie R 1963 *Electrochimica Acta* **8** 751–780

[16] De Levie R 1964 *Electrochimica acta* **9** 1231–1245

[17] Cruz-Manzo S and Greenwood P 2020 *Journal of Electroanalytical Chemistry* **871** 114305 ISSN 1572-6657

[18] Gaberscek M 2022 *Current Opinion in Electrochemistry* **32** 100917 ISSN 2451-9103

[19] Warburg E 1901 *Ann. Phys.* **311** 125–135

[20] Bard A J and Faulkner L R 2001 *Electrochemical Methods : Fundamentals and Application* 2nd ed (John Wiley and Sons)

[21] Schönleber M, Uhlmann C, Braun P, Weber A and Ivers-Tiffée E 2017 *Electrochimica Acta* **243** 250–259

[22] Devan S, Subramanian V R and White R E 2004 *Journal of The Electrochemical Society* **151** A905

[23] Sikha G and White R E 2007 *Journal of The Electrochemical Society* **154** A43

[24] Sikha G and White R E 2008 *Journal of the Electrochemical Society* **155** A893

[25] Huang J and Zhang J 2016 *Journal of the Electrochemical Society* **163** A1983

[26] Huang J, Gao Y, Luo J, Wang S, Li C, Chen S and Zhang J 2020 *Journal of the Electrochemical Society* **167** 166503

[27] Meyers J P, Doyle M, Darling R M and Newman J 2000 *Journal of The Electrochemical Society* **147** 2930

[28] Marinho B, Ghislandi M, Tkalya E, Koning C E and de With G 2012 *Powder Technology* **221** 351–358 ISSN 0032-5910 selected papers from 2010 AIChE Annual Meeting

[29] Profatilova I, De Vito E, Genies S, Vincens C, Gutel E, Fanget O, Martin A, Chandesris M, Tulodziecki M and Porcher W 2020 *ACS Applied Energy Materials* **3** 11873–11885

[30] Chaouachi O, Réty J M, Génies S, Chandesris M and Bultel Y 2021 *Electrochimica Acta* **366** 137428

[31] Subramanian V R and White R E 2001 *Journal of Power Sources* **96** 385–395 ISSN 0378-7753

[32] Evans J, Vincent C A and Bruce P G 1987 *Polymer* **28** 2324–2328

[33] Randles J E B 1947 *Discussions of the faraday society* **1** 11–19

[34] Huang J, Li Z, Zhang J, Song S, Lou Z and Wu N 2015 *Journal of The Electrochemical Society* **162** A585

[35] Kabir M and Demirocak D E 2017 *International Journal of Energy Research* **41** 1963–1986

A Full set of equations of the P2D model

Electrolyte

Within the framework of concentrated solutions theory, the equations for ionic charge and mass transport in the porous electrode are

$$\varepsilon\partial_t C_l = \nabla.\left(D_l^{\text{eff}}(C_l)\left(1+\frac{\partial \ln f(C_l)}{\partial \ln C_l}\right)\nabla C_l - t^+(C_l)\frac{i_l}{F}\right) + \frac{\nabla.i_l}{F} \tag{15}$$

$$i_l = -\sigma_l^{\text{eff}}(C_l)\nabla\varphi_l + \frac{2RT\sigma_l^{\text{eff}}(C_l)(1-t^+(C_l))}{F}\left(1+\frac{\partial \ln f(C_l)}{\partial \ln C_l}\right)\frac{\nabla C_l}{C_l} \tag{16}$$

where i_l [A/m^2] is the ionic current density, φ_l[V] is the electrochemical potential of Li^+ ions, $D_l^{\text{eff}} = D_l\frac{\varepsilon}{\tau}$ is the effective ionic diffusion coefficient and $\sigma_l^{\text{eff}} = \sigma_l\frac{\varepsilon}{\tau}$ is the effective ionic conductivity in the porous medium of the electrode. All transport coefficients $D_l^{\text{eff}}, \sigma_l^{\text{eff}}, t^+$ and the electrolyte activity f depends on the electrolyte concentration C_l. The Nernst-Einstein relation between D_l and σ_l is no longer valid for

concentrated solutions, so we define the non-dimensional coefficient α_l as the deviation from the Nernst-Einstein relation

$$D_l = \alpha_l \frac{2RT\sigma_l}{F^2 c_0} t^+(1-t^+)$$

The equation for charge conservation in the electrolyte is

$$\nabla . i_l = S_a \left(j_{out} + j_{dbl}\right) \tag{17}$$

where j_{out} [A/m^2] is the Li^+current flowing out of the particle and j_{dbl} [A/m^2] is the current for double layer charging.

A schematic representation of the porous electrode is displayed in Fig. 1. The boundary conditions are zero mass and charge flux at the current collector position $x = 0$

$$\begin{cases} -D_l^{\text{eff}} \nabla C_l + t^+ \frac{i_l}{F}\big|_{x=0} = 0 \\ i_l|_{x=0} = 0 \end{cases} \tag{18}$$

and conservation of the full current density I [A/m^2]crossing the electrode/separator interface located at $x = L$

$$i_l|_{x=L} = I \tag{19}$$

Solid phase

The lithium transport in active particles is modeled by the standard diffusion equation (Fick's law)

$$\partial_t C_s = \nabla . \left(D_s(C_s) \nabla C_s\right) \tag{20}$$

where C_s is the lithium concentration in the active matter, and $D_s(C_s)$ is the solid diffusion coefficient, that depends on the local lithium concentration. The boundary condition at the particle surface is

$$-D_s \mathbf{n}_{sl} . \nabla C_s = \frac{j_{out}}{F} \tag{21}$$

where $\mathbf{n}_{sl}$ is the unit vector pointing outwards.

Solid-electrolyte interface

The solid-electrolyte interface is modeled by the (non-linear) Butler-Volmer expression in parallel with a capacity representative of the electronic double-layer. The situation is represented in Fig. (7). The Butler-Volmer equation is

$$j_{out} = j_0(C_s(r)) \left(\frac{C_l}{c_0}\right)^{\alpha} \left[e^{\alpha \frac{F}{RT}\eta} - e^{-(1-\alpha)\frac{F}{RT}\eta}\right] \tag{22}$$

where $C_s(r)$ is the lithium concentration in solid phase at the particle surface, C_l is the ionic concentration in liquid phase at the particle surface, α is an empirical coefficient to quantify insertion/desinsertion asymmetric kinetics, and η is the insertion overpotential given by

$$\eta = \Phi - \phi_{ocv}(C_s(r)) - \varphi_l \tag{23}$$

with Φ the electric potential, $\phi_{ocv}(C_s(r))$ is the equilibrium potential of the active material at the lithium concentration $C_s(r)$, and φ_l is the ionic electrochemical potential at the particle surface.

The equation for double-layer charging can be simply written

$$j_{dbl} = C_{dbl} \partial_t \left(\Phi - \varphi_l\right) \tag{24}$$

B Notations and symbols

The following tables 3 and 4 gather the different notations used in the manuscript. The parameters values used in the simulations for the active materials graphite, NMC and LFP are given in table 3, and for the electrolyte in table 4.

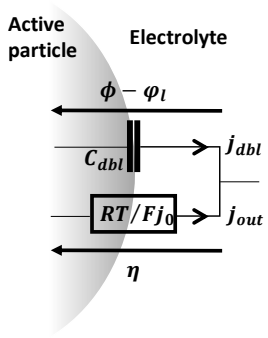

Figure 7: Representation of the interface kinetics with double-layer charging.

Active material and electrode parameter	**Notation / units**	**Graphite**	**NMC**	**LFP**
OCV derivative vs stoechiometry	ϕ'_{ocv} [V]	-1	-1	-10
maximal concentration	c_s^{max} [mol/m^3]	30500	48000	23500
particle mean radius	r [μm]	8	2,5	0,1
solid diffusion coefficient	D_s [m^2/s]	10^{-14}	10^{-13}	10^{-16}
exchange current density	j_0 [A/m^2]	1	1,5	0,05
double-layer capacity	C_{dbl} [F/m^2]	0,62	0,093	0,093
porosity	ε	0,3	0,25	0,3
tortuosity	τ	7	2,5	2
thickness	L [μm]	80	60	110
exchange surface density	S_a [m^{-1}]	$\frac{3(1-\varepsilon)}{r}$	$\frac{3(1-\varepsilon)}{r}$	$\frac{3(1-\varepsilon)}{r}$

Table 3: Electrode parameters used in the present work. The exchange surface density S_a corresponds to identical spherical particles of radius r. The parameter values chosen for the electrode design, and for the active materials NMC, graphite and LFP are orders of magnitude at 25°C, and should not be considered as precise experimental values. The reader is referred to the open database *liiondb.com* for the various parameter values found in the literature.

Electrolyte parameter	**Notation / units**	**Value**
mean concentration	c_0 [mol/m^3]	1000
conductivity	σ_l [S/m]	1
transport number	t^+	0.3
ionic diffusion coefficient	D_l [m^2/s]	$1,12.10^{-10}$
Nernst-Einstein correction factor	α_l	1
activity factor	$\frac{\partial \ln \gamma}{\partial \ln c}$	0

Table 4: Electrolyte parameters used in the present work. The chosen values are typical orders of magnitude for a liquid electrolyte at 25°C.

C Particle impedance

This section presents in details the computation of the impedance Z_{part} of an individual particle defined by the relation Eq. (1), the derivation of the non-dimensional number N_s and the characteristic frequencies f_s and f_{capa} given in Table 1.

Lithium concentration in solid phase

The solid diffusion equation is given by Eq. (20). We decompose the concentration field in the vicinity of an equilibrium state of uniform concentration c_s^0 by $C_s = c_s^0 + c_s$, with the concentration fluctuation satisfying $c_s \ll c_s^0$. The full non-linear diffusion equation can be linearized in the vicinity of c_s^0 and gives to leading order

$$\partial_t c_s = D_s \Delta c_s \tag{25}$$

where $D_s = D_s(c_s^0)$ is a constant.

The active material is composed of identical spherical particles of radius r.

We thus proceed with Eq.(25) by writing the diffusion equation in spherical coordinates for the lithium concentration profile $c_s(y,t)$

$$\partial_t c_s = D_s \frac{1}{y} \frac{\partial^2}{\partial y^2} (y c_s) \tag{26}$$

with the boundary condition deduced from Eq. (21)

$$\begin{cases} -D_s \partial_y c_s(r,t) = \frac{j_{out}}{F} & \text{at the particle surface} \\ -D_s \partial_y c_s(r,t) = 0 & \text{at the particle center} \end{cases} \tag{27}$$

where j_{out} [A/m^2] is the current density flowing outwards the particle.

Eq. (26) can be solved by introducing the variable $z(y,t) = y c_s(y,t)$ and taking the time Fourier transform. We get the equation

$$i\omega z = D_s \frac{\partial^2 z}{\partial y^2}$$

Considering that the concentration is finite at the particle center, we have $z(y=0) = 0$, and the general solution is

$$z(y) = A \sinh\left(y \sqrt{\frac{i\omega}{D_s}} \right). \tag{28}$$

The integration constant A is found using the boundary condition Eq. (27)

$$-D_s \left[-\frac{z(r)}{r^2} + \frac{1}{r} \frac{\partial z}{\partial y}(r) \right] = \frac{j_{out}}{F}$$

$$-AD_s \left[-\frac{\sinh\left(r\sqrt{\frac{i\omega}{D_s}} \right)}{r^2} + \sqrt{\frac{i\omega}{D_s}} \frac{\cosh\left(r\sqrt{\frac{i\omega}{D_s}} \right)}{r} \right] = \frac{j_{out}}{F}$$

which gives

$$A = \frac{j_{out}}{FD_s} \frac{r^2}{\sinh\left(r\sqrt{\frac{i\omega}{D_s}} \right) - r\sqrt{\frac{i\omega}{D_s}} \cosh\left(r\sqrt{\frac{i\omega}{D_s}} \right)}. \tag{29}$$

As will be seen in the next section, the computation of Z_{part} requires to know the concentration at the particle surface $c_s(r)$. Its expression is given with the combination of Eqs. (28-29), using $c_s(y) = \frac{z(y)}{y}$:

$$c_s(r) = \frac{j_{out} r}{FD_s} \frac{\tanh(k_p r)}{\tanh(k_p r) - k_p r} \tag{30}$$

with the inverse of the diffusion length $k_p = \sqrt{i\omega / D_s}$.

Lithium insertion at the particle surface

The solid/electrolyte interface is modeled by Eqs. (22-23-24). It can be noticed that, while the Eq. (24) is linear, the Butler-Volmer Eq. (22) is not. The equilibrium state is reached for the electrode potential $\Phi^0 = \phi_{ocv}(c_s^0) + \varphi_l^0$. Without loss of generality, we choose the equilibrium potential such that $\varphi_l^0 = 0$. We consider a small fluctuation $\phi = \Phi - \Phi^0$ with $\phi \ll \frac{RT}{F}$, $\varphi_l \ll \frac{RT}{F}$, and $c_s(r) \ll c_s^0$ in the vicinity of this equilibrium state, and we expand the overpotential η of Eq.(23) to first perturbation order as

$$\begin{aligned}\eta &= \Phi^0 + \phi - \phi_{ocv}(c_s^0 + c_s(r)) - \varphi_l \\ &= \phi_{ocv}(c_s^0) + \phi - \left[\phi_{ocv}(c_s^0) + \frac{\mathrm{d}\phi_{ocv}}{\mathrm{d}c_s} c_s(r)\right] - \varphi_l \\ &\approx \phi - \frac{\mathrm{d}\phi_{ocv}}{\mathrm{d}c} c_s(r) - \varphi_l\end{aligned}$$

The assumption that $\eta \ll \frac{RT}{F}$ then allows to expend the exponential terms in Eq. (22) to leading order as

$$e^{\alpha \frac{F}{RT}\eta} - e^{-(1-\alpha)\frac{F}{RT}\eta} \approx \frac{F}{RT}\left(\phi - \frac{\mathrm{d}\phi_{ocv}}{\mathrm{d}c_s} c_s(r) - \varphi_l\right)$$

Finally, we notice that the expansions of the nonlinear prefactors $j_0(C_s(r))$ and $\left(\frac{c_l}{c_0}\right)^\alpha$ to first order would only add second order corrections to the Butler-Volmer Eq. (22). The linear Butler-Volmer equation is thus to leading order

$$j_{out} = \frac{j_0 F}{RT}\left(\phi - \frac{\mathrm{d}\phi_{ocv}}{\mathrm{d}c_s} c_s(r) - \varphi_l\right) \tag{31}$$

where $j_0 = j_0(c_s^0)$ is the exchange current value at the equilibrium concentration c_s^0.

Particle impedance

Once the surface lithium concentration c_s is known from Eq.(30), we can close the Eq.(31) to express the lithium insertion flux j_{out} as

$$\begin{aligned} j_{out} &= \frac{j_0 F}{RT}\left(\phi - \frac{\mathrm{d}\phi_{ocv}}{\mathrm{d}c_s}\frac{j_{out} r}{F D_s}\frac{\tanh(k_p r)}{\tanh(k_p r) - k_p r} - \varphi_l\right) \\ j_{out}\left(1 + \frac{\mathrm{d}\phi_{ocv}}{\mathrm{d}c_s}\frac{j_0 r}{RT D_s}\frac{\tanh(k_p r)}{\tanh(k_p r) - k_p r}\right) &= \frac{j_0 F}{RT}\left(\phi - \varphi_l\right) \\ j_{out}\left(1 + Z_s\right) &= \frac{j_0 F}{RT}\left(\phi - \varphi_l\right) \end{aligned} \tag{32}$$

where we have introduced the non-dimensional solid diffusion impedance Z_s given by

$$Z_s = \frac{\mathrm{d}\phi_{ocv}}{\mathrm{d}c_s}\frac{j_0 r}{RT D_s}\frac{\tanh(k_p r)}{\tanh(k_p r) - k_p r}$$

The OCV derivative is usually given with respect to the stoechiometry x_{Li} using $c_s = x_{Li} c_s^{\max}$. Furthermore, the OCV always decreases when the lithium concentration increases such that $\phi'_{ocv} = -|\phi'_{ocv}| < 0$ for all active materials. We thus write

$$\frac{\mathrm{d}\phi_{ocv}}{\mathrm{d}c_s} = -\frac{|\phi'_{ocv}|}{c_s^{\max}}$$

Using then the expression of the non-dimensional number N_s and the solid frequency f_s, both given in Table 1, one can find the solid diffusion impedance expression (see Eq. (4)) [31, 8]

$$Z_s = N_s \frac{\tanh(\sqrt{i\omega/f_s})}{\sqrt{i\omega/f_s} - \tanh(\sqrt{i\omega/f_s})} \tag{33}$$

The charge conservation law for the electrolyte is

$$\nabla . i_l = S_a\left(j_{out} + j_{dbl}\right) \tag{34}$$

Using Eq.(32) and the time Fourier transform of Eq.(24), the charge conservation becomes

$$\nabla.i_l = \frac{S_a j_0 F}{RT}\left(\frac{1}{1+Z_s} + \frac{i\omega}{2\pi f_{capa}}\right)(\phi - \varphi_l)$$

$$\frac{\nabla.i_l}{S_a}\frac{RT}{Fj_0}\left(\frac{1+Z_s}{1+\frac{i\omega}{2\pi f_{capa}}(1+Z_s)}\right) = \phi - \varphi_l \tag{35}$$

with the double-layer charging frequency given by $f_{capa} = \frac{Fj_0}{2\pi RTC_{dbl}}$. Note that we have used the equality $\partial_t\Phi = \partial_t\phi$ because the equilibrium potential $\phi_{ocv}(c_s^0)$ does not depend on time. The particle total impedance is finally given by (see also Eq.(10))

$$Z_{part} = \frac{R_{CT}}{\frac{1}{1+Z_s} + i\frac{\omega}{2\pi f_{capa}}}. \tag{36}$$

with the charge transfer resistance $R_{CT} = \frac{RT}{Fj_0}$. This expression corresponds to the classical Randles circuit impedance combining solid diffusion and charge transfer [33, 21].

D Non-dimensional set of equations

We give in this section the derivation of the non-dimensional set of equations for the transport equations in the electrolyte, in the linear regime. The full set of equations is given in Eqs. (15-16).

The equilibrium state is reached for a constant uniform concentration $C_l^0 = c_0$, no currents $i_l^0 = 0$ and constant ionic potential $\varphi_l^0 = 0$. We consider a small perturbation $C_l = c_0 + c_l$ with $c_l \ll c_0$, $\varphi_l \ll \frac{RT}{F}$ and $i_l \ll j_0$ in the vicinity of this equilibrium state. The expansion of Eqs. (15-16) to first order gives

$$\varepsilon\partial_t c_l = \nabla.\left(D_l^{\text{eff}}.\left(1 + \frac{\partial \ln f}{\partial \ln c}\right)\nabla c_l + t^+\frac{i_l}{F}\right) + \frac{\nabla i_l}{F} \tag{37}$$

$$i_l = -\sigma_l^{\text{eff}}\nabla\varphi_l + \frac{2RT\sigma_l^{\text{eff}}(1-t^+)}{Fc_0}\left(1 + \frac{\partial \ln f}{\partial \ln c}\right)\nabla c_l \tag{38}$$

where the transport coefficients $D_l^{\text{eff}}, \sigma_l^{\text{eff}}, t^+$ and the activity coefficient $\frac{\partial \ln f}{\partial \ln c}$ should be evaluated at the equilibrium concentration c_0 and considered as constants.

We proceed by introducing the non-dimensional set of variables

$$\begin{cases} \widetilde{c}_l &= \frac{c_l}{c_0} \\ \widetilde{i}_l &= \frac{\lambda i_l}{Fc_0 D_l^{\text{eff}}\left(1+\frac{\partial \ln f}{\partial \ln c}\right)} \\ \widetilde{\varphi}_l &= \frac{F\varphi_l}{RT} \end{cases} \tag{39}$$

and the non-dimensional space variable $\widetilde{x} = \frac{x}{\lambda}$, where the penetration length λ is given by

$$\lambda = \sqrt{\frac{RT\sigma_l^{\text{eff}}}{Fj_0 S_a}} \tag{40}$$

The time Fourier transform of Eqs. (37-38) gives

$$\frac{\lambda^2\varepsilon}{D_l^{\text{eff}}\left(1+\frac{\partial \ln f}{\partial \ln c}\right)} i\omega\widetilde{c}_l = \widetilde{c}_l'' + (1-t^+)\widetilde{i}_l' \tag{41}$$

$$\widetilde{i}_l = -\frac{\widetilde{\varphi}_l'}{2\alpha_l t^+(1-t^+)\left(1+\frac{\partial \ln f}{\partial \ln c}\right)} + \frac{\widetilde{c}_l'}{\alpha_l t^+} \tag{42}$$

with the prime denoting the spatial derivative wrt $\widetilde{x}$. It can be seen with this non-dimensional choice of variables, that the characteristic ionic diffusion frequency f_{el} given by Eq. (6) naturally appears in the set of equations as the unique timescale of electrolyte transport. The electrolyte potential and current density are related by Eq. (35). Using the non-dimensional variables given in Eq. (39), this relation becomes

$$\widetilde{Z}_{part}\widetilde{i}_l' = \frac{\tilde{\phi} - \widetilde{\varphi}_l}{2\alpha_l t^+(1-t^+)\left(1+\frac{\partial \ln f}{\partial \ln c}\right)} \tag{43}$$

The latter relation can be derived to replace the potential derivative in Eq. (42). As the electric potential do not depend on space, we get $\tilde{\phi}' = 0$ and the final set of equations are

$$i\frac{\omega}{2\pi f_{el}}\widetilde{c}_l = \widetilde{c}_l'' + (1-t^+)\widetilde{i}_l' \tag{44}$$

$$\widetilde{i}_l = \widetilde{Z}_{part}\widetilde{i}_l'' + \frac{\widetilde{c}_l'}{\alpha_l t^+} \tag{45}$$

with $\widetilde{Z}_{part} = \frac{Fj_0}{RT}Z_{part}$. This set of equations should be solved for both electrodes positive and negative, with the proper boundary conditions at the interfaces with the separator. This is done in the next section.

E Analytical resolution

Computation of the eigenvalues and eigenmatrix

We solve in this section the set of Eqs.(44-45) using an eigenmodes decomposition. For clarity, we omit the tilt on the variables such that the calculations below should always be understood with the non-dimensional fields except otherwise stated.

The boundary condition at the interface with the current collector, located at $x = 0$ are zero mass and charge fluxes. We thus look for a solution of the system of Eqs.(44-45) in the form

$$\begin{pmatrix} c_l \\ i_l \end{pmatrix} = \begin{pmatrix} a\cosh(kx) \\ b\sinh(kx) \end{pmatrix} \tag{46}$$

where a, b are constants to be determined, and k is an eigenvalue. With the ansatz Eq.(46), the system (44-45) becomes

$$\left[a\left(k^2 - i\frac{\omega}{2\pi f_{el}}\right) + bk(1-t^+)\right]\cosh(kx) = 0$$
$$\left[b\left(k^2 Z_{part} - 1\right) + \frac{ak}{\alpha_l t^+}\right]\sinh(kx) = 0$$

The above system has a non-trivial solution if the system discriminant is zero, which means that k satisfies the equation

$$\left(k^2 - i\frac{\omega}{2\pi f_{el}}\right)\left(k^2 Z_{part} - 1\right) - \frac{k}{\alpha_l t^+}k(1-t^+) = 0$$

or equivalently

$$Z_{part}k^4 - \left(\frac{i\omega}{2\pi f_{el}}Z_{part} + N_{el}\right)k^2 + i\frac{\omega}{2\pi f_{el}} = 0 \tag{47}$$

The Eq.(47) has four solutions, but the solutions k and $-k$ are physically equivalent. Let then k_1, k_2 be the two independent solutions of Eq.(47), such that $k_1^2 \underset{\omega\to+\infty}{\sim} \frac{i\omega}{2\pi f_{el}}$ and $k_2^2 \underset{\omega\to+\infty}{\sim} \frac{1}{Z_{part}}$. For k satisfying the eigenvalue equation, the constants a and b are related by

$$a\left(k^2 - i\frac{\omega}{2\pi f_{el}}\right) = -bk(1-t^+) \tag{48}$$

Let α be the constant related to the first eigenmode of eigenvalue k_1, the relation Eq. (48) is satisfied by setting

$$\begin{cases} a &= -\alpha k_1(1-t^+) \\ b &= \alpha\left(k_1^2 - i\frac{\omega}{2\pi f_{el}}\right) \end{cases} \tag{49}$$

An equivalent relation holds with the constant β related to the eigenmode of eigenvalue k_2. The general solution (c_l, i_l) can be written as the linear combination of the two eigenmodes defined by Eqs. (46-49)

$$\begin{aligned} \begin{pmatrix} c_l \\ i_l \end{pmatrix} &= \begin{pmatrix} -k_1(1-t^+)\cosh(k_1 x) & -k_2(1-t^+)\cosh(k_2 x) \\ \left(k_1^2 - i\frac{\omega}{2\pi f_{el}}\right)\sinh(k_1 x) & \left(k_2^2 - i\frac{\omega}{2\pi f_{el}}\right)\sinh(k_2 x) \end{pmatrix} . \begin{pmatrix} \alpha \\ \beta \end{pmatrix} \\ \begin{pmatrix} c_l \\ i_l \end{pmatrix} &= A(x) . \begin{pmatrix} \alpha \\ \beta \end{pmatrix} \end{aligned} \tag{50}$$

where we have introduced $A(x)$ the eigenmodes matrix of the system.

The next step is to relate the constants (α, β) to the boundary conditions at the interface with the separator. Let assume that we are dealing with the positive electrode, and let $x = L_p$ be the location of the electrode-separator interface (see Fig. 1). We have the two constrains

$$\begin{cases} c_l(L_p) &= c_p \\ i_l(L_p) &= I_p \end{cases}$$

where $c_p$is the concentration on top of the electrode (unknown), and I_p is the (non-dimensional) total current outwards the electrode The value of $I_p$is related to the total current density I $[A/m^2]$ imposed to the cell by

$$I_p = \frac{\lambda_p I}{F c_0 D_p^{\text{eff}}\left(1 + \frac{\partial \ln f}{\partial \ln c}\right)} \tag{51}$$

according to the adimensionalization of Eq.(39), where D_p^{eff} is the value of D_l^{eff} for the positive electrode, and λ_p is the penetration length of the positive. From Eq.(50) we have the relation

$$A(L_p) . \begin{pmatrix} \alpha \\ \beta \end{pmatrix} = \begin{pmatrix} c_p \\ I_p \end{pmatrix}$$

The general solution can thus be expressed as

$$\begin{aligned} \begin{pmatrix} c_l \\ i_l \end{pmatrix} &= A(x).A^{-1}(L_p) \begin{pmatrix} c_p \\ I_p \end{pmatrix} \\ \begin{pmatrix} c_l \\ i_l \end{pmatrix} &= M(x) . \begin{pmatrix} c_p \\ I_p \end{pmatrix} \end{aligned} \tag{52}$$

where we have introduced the new matrix $M(x) = A(x).A^{-1}(L_p)$. There exists another matrix $N(x)$ for the negative electrode such that the fields (c_l, i_l) in the negative are given by

$$\begin{pmatrix} c_l \\ i_l \end{pmatrix} = N(x) . \begin{pmatrix} c_n \\ I_n \end{pmatrix} \tag{53}$$

The computation of $N(x)$ is completely similar to that of the positive electrode described above.

Continuity relations at the interfaces

The next step is to compute the unknown concentrations values c_p and c_n at the two interfaces between the electrodes and the separator. They can be found by expressing the continuity of mass transport between the two electrodes and the separator. This is done by enforcing the continuity of the mass flux

$-D_l^{\text{eff}}\left(1+\frac{\partial \ln f}{\partial \ln c}\right)\nabla c_l$ at the interfaces. In the present section, we come back to dimensional variables, and we write with a tild the non-dimensional ones.

The mass flux at the interface between the positive and the separator can be expressed as

$$-D_p^{\text{eff}}\left(1+\frac{\partial \ln f}{\partial \ln c}\right)\frac{\partial c_l}{\partial x}(L_p) = -D_p^{\text{eff}}\left(1+\frac{\partial \ln f}{\partial \ln c}\right)\frac{c_0}{\lambda_p}\frac{\partial \widetilde{c}_l}{\partial \widetilde{x}}(L_p) \tag{54}$$

Using the matrix of eigenvectors $M(x)$ given by Eq.(52), the concentration derivative in Eq.(54) can be written

$$-D_p^{\text{eff}}\left(1+\frac{\partial \ln f}{\partial \ln c}\right)\frac{\partial c_l}{\partial x}(L_p) = -D_p^{\text{eff}}\left(1+\frac{\partial \ln f}{\partial \ln c}\right)\frac{c_0}{\lambda_p}\left(\widetilde{c}_p M'_{11}(\widetilde{L}_p)+\widetilde{I}_p M'_{12}(\widetilde{L}_p)\right) \tag{55}$$

where we have introduced the derivative $M'(x)=\frac{\partial A(x)}{\partial x}.A^{-1}(\widetilde{L}_p)$. Using the same procedure for the negative electrode, the mass flux at the interface with the separator can be expressed as

$$-D_n^{\text{eff}}\left(1+\frac{\partial \ln f}{\partial \ln c}\right)\frac{\partial c_l}{\partial x}(L_n) = -D_n^{\text{eff}}\left(1+\frac{\partial \ln f}{\partial \ln c}\right)\frac{c_0}{\lambda_n}\left(-\widetilde{c}_n M'_{11}(\widetilde{L}_n)+\widetilde{I}_n M'_{12}(\widetilde{L}_n)\right) \tag{56}$$

Please note that the sign of $-\widetilde{c}_n$ in Eq. (56) comes from the fact that the negative electrode is reversed compared to the positive electrode.

We do not display the computation of the mass flux inside the separator, as it can be obtained straightforward by solving the diffusion equation in the electrolyte Eq.(15) without source terms. Let l be the separator width, and

$$\xi^2 = \frac{\varepsilon_{sep}\omega}{D_{sep}^{\text{eff}}}$$

be characteristic diffusion length inside the separator. The mass continuity at the two interfaces is given by the system

$$\begin{cases} -D_p^{\text{eff}}\left(1+\frac{\partial \ln f}{\partial \ln c}\right)\frac{c_0}{\lambda_p}\left(\widetilde{c}_p M'_{11}(\widetilde{L}_p)+\widetilde{I}_p M'_{12}(\widetilde{L}_p)\right) & = -D_{sep}^{\text{eff}}\left(1+\frac{\partial \ln f}{\partial \ln c}\right)\frac{\xi c_0}{\sinh(\xi l)}\left(\widetilde{c}_n-\widetilde{c}_p\cosh(\xi l)\right) \\ -D_n^{\text{eff}}\left(1+\frac{\partial \ln f}{\partial \ln c}\right)\frac{c_0}{\lambda_n}\left(-\widetilde{c}_n N'_{11}(\widetilde{L}_n)+\widetilde{I}_n N'_{12}(\widetilde{L}_n)\right) & = -D_{sep}^{\text{eff}}\left(1+\frac{\partial \ln f}{\partial \ln c}\right)\frac{\xi c_0}{\sinh(\xi l)}\left(\widetilde{c}_n\cosh(\xi l)-\widetilde{c}_p\right) \end{cases}$$

or equivalently

$$\begin{cases} \left(-M'_{11}(\widetilde{L}_p)-\frac{D_{sep}^{\text{eff}}}{D_p^{\text{eff}}}\frac{\lambda_p\xi}{\tanh(\xi l)}\right)\widetilde{c}_p+\frac{D_{sep}^{\text{eff}}}{D_p^{\text{eff}}}\frac{\lambda_p\xi}{\sinh(\xi l)}\widetilde{c}_n & = \widetilde{I}_p M'_{12}(\widetilde{L}_p) \\ -\frac{D_{sep}^{\text{eff}}}{D_n^{\text{eff}}}\frac{\lambda_n\xi}{\sinh(\xi l)}\widetilde{c}_p+\left(N'_{11}(\widetilde{L}_n)+\frac{D_{sep}^{\text{eff}}}{D_n^{\text{eff}}}\frac{\lambda_n\xi}{\tanh(\xi l)}\right)\widetilde{c}_n & = \widetilde{I}_n N'_{12}(\widetilde{L}_n) \end{cases} \tag{57}$$

The set of equations Eq.(57) can be solved to find the two boundary concentrations c_p, c_n as function of the applied current. This last step completely solves the problem. It can be seen from Eq.(51) that $\widetilde{I}_p$and $\widetilde{I}_n$ are both proportional to I, and thus c_p, c_n are also proportional to I by linearity.

Computation of the impedance

The individual particle impedance is known from Eq.(36). The electrolyte concentration and current fields can be computed by the eigenmodematrices M and N given by Eqs.(52-53). The interfaces concentrations are computed from the linear system Eq.(57). The only remaining step is to express the positive and negative impedances from the current and potential fields.

The electrode positive impedance should be understood as the difference between the uniform electric potential of the electrode and the ionic electrochemical potential on top of the electrode $\phi-\varphi_l(L_p)$, divided by the current density

$$\begin{aligned} Z^+ &= \frac{\phi-\varphi_l(L_p)}{I} \\ &= \frac{\lambda_p}{\sigma_p^{\text{eff}}}\frac{1}{2\alpha_l t^+(1-t^+)\left(1+\frac{\partial \ln f}{\partial \ln c}\right)}\frac{\widetilde{\phi}-\widetilde{\varphi}_l(\widetilde{L}_p)}{\widetilde{I}_p} \end{aligned}$$

Using the relation Eq.(43) to replace the potential, we get

$$Z^+ = \frac{\lambda_p}{\sigma_p^{\text{eff}}} \widetilde{Z}^+_{part}. \frac{\widetilde{i}'_l(\widetilde{L}_p)}{\widetilde{I}_p}$$
$$Z^+ = \frac{\lambda_p}{\sigma_p^{\text{eff}}} \widetilde{Z}^+_{part}. \left(M'_{22}(\widetilde{L}_p) + \frac{\widetilde{c}_p}{\widetilde{I}_p} M'_{21}(\widetilde{L}_p) \right) \tag{58}$$

The following similar relation holds for the negative electrode impedance

$$Z^- = \frac{\lambda_n}{\sigma_n^{\text{eff}}} \widetilde{Z}^-_{part}. \left(N'_{22}(\widetilde{L}_n) - \frac{\widetilde{c}_n}{\widetilde{I}_n} N'_{21}(\widetilde{L}_n) \right) \tag{59}$$

In an experimental setup, the impedance contribution of the separator cannot be separated from that of the electrode, and should be included in the computation of the total positive and negative impedance. The positive and negative impedances of the cell are defined from the potential drop between the current collector and the middle of the separator, as represented in Fig. 1. We do not detail the calculation, it can be done straightforward from the resolution of the charge transport equation in the separator. We get for the positive

$$Z_{pos} = Z^+ + \frac{l}{2\sigma_{sep}^{\text{eff}}} + \frac{\lambda_p}{\alpha_l t^+ \sigma_p^{\text{eff}}} \frac{1}{\widetilde{I}_p} \left(\widetilde{c}_p - \frac{\widetilde{c}_p + \widetilde{c}_n}{2\cosh(\xi l/2)} \right) \tag{60}$$

and for the negative

$$Z_{neg} = Z^- + \frac{l}{2\sigma_{sep}^{\text{eff}}} + \frac{\lambda_n}{\alpha_l t^+ \sigma_n^{\text{eff}}} \frac{1}{\widetilde{I}_n} \left(\frac{\widetilde{c}_p + \widetilde{c}_n}{2\cosh(\xi l/2)} - \widetilde{c}_n \right) \tag{61}$$

F Negligible electrolyte diffusion limit

The negligible electrolyte diffusion limit corresponds to $t^+ \to 1$ in Eqs. (44-45). The source term in the mass transport Eq. (44) disappears, which means that the electrolyte concentration profile remains uniform. The limit can be interpreted as that of vanishing anions mobility. If the anions can't move, the lithium ion concentration profile can't be distorted because it would break electroneutrality.

The charge transport equation is then

$$i_l = \lambda^2 \frac{F j_0}{RT} Z_{part} i''_l$$

with the boundary conditions

$$\begin{cases} i_l(x=0) = 0 & \text{at the electrode-collector interface} \\ i_l(x=L) = I & \text{at the electrode-separator interface} \end{cases}$$

The solution is

$$i_l(x) = I \frac{\sinh\left(\frac{x}{\lambda \sqrt{\frac{F j_0}{RT} Z_{part}}} \right)}{\sinh\left(\frac{L}{\lambda \sqrt{\frac{F j_0}{RT} Z_{part}}} \right)} \tag{62}$$

The relation (35) allows to express the potential difference from the electrolyte current density by

$$\frac{\nabla . i_l}{S_a} Z_{part} = \phi - \varphi_l \tag{63}$$

and the electrode impedance is then simply given by

$$Z = \frac{\phi - \varphi_l(L)}{I}$$

Using Eqs. (62) and (63) we get

$$Z = \frac{Z_{part}}{S_a \lambda \sqrt{\frac{F j_0}{RT} Z_{part}}} \frac{1}{\tanh\left(\frac{L}{\lambda\sqrt{\frac{F j_0}{RT} Z_{part}}}\right)}$$
$$= \frac{\lambda}{\sigma_l^{\text{eff}}} \frac{\sqrt{\frac{F j_0}{RT} Z_{part}}}{\tanh\left(\frac{L}{\lambda\sqrt{\frac{F j_0}{RT} Z_{part}}}\right)}$$

which is the distributed particle impedance given by Eq. (10).

G low frequency limit of the electrolyte diffusion

In the present section, we give the analytic expression for the vanishing frequency limit $f \to 0$ of the P2D model, with negligible solid diffusion. This limit can be achieved with $\phi'_{ocv} = 0$, because the solid diffusion has no contribution in the overpotential. The solid diffusion impedance is $Z_s = 0$.

It should first be noted from Eq. (36) that

$$Z_{part} \underset{f\to 0}{\longrightarrow} \frac{RT}{F j_0} \tag{64}$$

Imposing this limit in Eqs. (37-38), with $\omega = 0$, gives

$$\widetilde{c}_l'' = -(1-t^+)\widetilde{i}_l' \tag{65}$$
$$\widetilde{i}_l = \widetilde{i}_l'' + \frac{\widetilde{c}_l'}{\alpha_l t^+} \tag{66}$$

Integrating Eq. (65) with the boundary condition at the current collector interface $\widetilde{c}_l'(0) = 0$ gives

$$\widetilde{c}_l' = -(1-t^+)\widetilde{i}_l$$

and using this result in Eq. (66) gives a close equation for $\widetilde{i}_l$

$$\widetilde{i}_l'' = \widetilde{i}_l \left(1 + \frac{1-t^+}{\alpha_l t^+}\right)$$
$$\widetilde{i}_l'' = N_{el} \widetilde{i}_l \tag{67}$$

The solution of Eq. (67) with vanishing current density at the collector, and $i_l = I$ is (with dimensional variables)

$$i_l = I \frac{\sinh\left(\sqrt{N_{el}}\frac{x}{\lambda}\right)}{\sinh\left(\sqrt{N_{el}}\frac{L}{\lambda}\right)} \tag{68}$$

Once the current density is found, the electrode impedance can be computed straightforward using the same equations as in appendix F, and gives

$$Z \underset{f\to 0}{\longrightarrow} \frac{\lambda}{\sigma_l^{\text{eff}}} \frac{\sqrt{N_{el}}}{\tanh\left(\sqrt{N_{el}}\frac{L}{\lambda}\right)}$$

From that expression, R_l in Eq. (13) can be computed by subtracting the low frequency limit of the TLM impedance. The low-frequency limit of the separator impedance can be computed straightforward using the mass and charge transport equations without source terms, and the continuity relations for i_l and $D_l^{\text{eff}} \nabla c_l$ at the electrode interfaces.